

Metamaterial as a controllable template for nanoscale field localization

T. S. Kao,^{1,a)} F. M. Huang,¹ Y. Chen,² E. T. F. Rogers,¹ and N. I. Zheludev¹

¹Optoelectronics Research Centre, University of Southampton, Southampton, Hampshire SO17 1BJ, United Kingdom

²Rutherford Appleton Laboratory, Chilton, Didcot, Oxon OX11 0QX, United Kingdom

(Received 26 October 2009; accepted 21 December 2009; published online 27 January 2010)

We report that subwavelength localization of light in the near-field of a double-periodic photonic metamaterial may be efficiently controlled by the polarization and wavelength of the incident radiation. A dramatic variation in the periodic near-field landscapes, including a transition from a pattern of isolated subwavelength plasmon hot-spots to a blurred, low contrast pattern, accompanied by a change in the pattern's symmetry has been observed in the proximity of an aluminum nanowire “fish-scale” nanostructure. Hot-spots as small as 0.23λ have been achieved and their position has been controlled by tuning the wavelength of incident light across the dipole absorption resonance of the metamaterial. A simple switch of the polarization state can lead to a spatial period doubling in the landscape pattern. © 2010 American Institute of Physics. [doi:10.1063/1.3291675]

Metamaterials constructed from artificial metallic nanostructures exhibit unusual electromagnetic properties such as extraordinary transmission of light through subwavelength hole arrays,^{1,2} negative refraction,^{3,4} local field enhancement,^{5,6} and subwavelength concentration of light beyond the near-field.^{7,8} Here we will demonstrate another application of metamaterial nanostructures, in this case for controllable templating of nanostructured optical field localization. A double-periodic subwavelength “fish-scale” nanowire structure, a metamaterial with period smaller than the wavelength of light, will be used as an example. This structure manifests rich resonant electromagnetic properties. When mounted on a metal backing plate, it acts as “magnetic mirror” reversing the magnetic field of the incident wave upon reflection.^{9,10} Such a structure acts as a local field concentrator and a resonant “amplifier” of losses in the underlying dielectric.⁹ Tilted fish-scale patterns that lack a plane of symmetry belong to the category of planar chiral structures and show asymmetric transmission of light in opposite directions¹¹ and support enantiomeric sensitive plasmon excitations.^{12,13}

The far-field metamaterial properties listed above are due to the plasmonic response of the structure. However, plasmonic excitations in such structures have never been studied experimentally before and only limited data exist on the study of near-field and plasmon localization in metamaterials.^{14,15} Plasmons can be mapped with nanoscale resolution using cathodoluminescence¹⁶ and scanning near-field optical microscopy (SNOM). Although justifiable concerns have been raised regarding the disturbance that the SNOM tip could cause to the near-field of the investigated structure,^{17,18} SNOM provides a powerful and informative tool for mapping plasmon fields.^{15,19,20} Indeed our measurements illustrate that a good qualitative agreement is seen between the field maps measured by the SNOM technique and computed theoretically.

Here we report the observation of subwavelength localization of plasmons in a double-periodic photonic metamaterial, an aluminum nanowire “fish-scale” pattern supported by

a dielectric substrate, illuminated by a coherent light source. We show that the plasmon landscape can be efficiently controlled by the polarization and wavelength of the incident radiation.

A schematic diagram of the experimental configuration and nanostructure of the metamaterial samples are shown in Fig. 1. Aluminum nanowires of approximately 50 nm thickness and 50 nm width were fabricated using electron-beam lithography on a 500 μm thick transparent silica substrate. The metamaterial samples consisted of a double-periodic round “fish-scale” pattern with a $440 \times 440 \text{ nm}^2$ unit-cell. The metamaterial structure contained about 1.2×10^6 fish-scale unit cells and had lateral dimensions of $500 \times 500 \mu\text{m}^2$. For field mapping we used a scanning near-field optical microscope (SNOM) (Omicron Co., Twin-SNOM) in transmission mode employing polarization-insensitive metal-coated SNOM tapered fiber probes (Jasco Inc.) with 60 nm aperture. To study the field distributions at different excitation wavelengths the samples were illuminated with a super-continuum laser source (Fianium Co., SC450-2) through bandpass spectral filters. This was complemented by normal incidence far-field transmission measurements in the range between 500 and 900 nm using a microspectrophotometer (CRAIC Tech., QDI 2010).

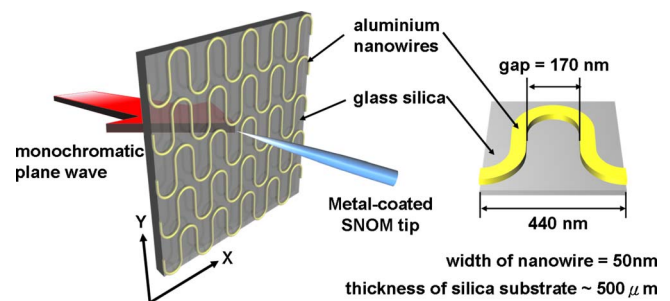


FIG. 1. (Color online) Mapping near-fields of the nanowire array. Schematic diagram of experimental configuration. The near-field intensity distributions of double-periodic nanowire arrays were directly measured under monochromatic plane wave illumination, using a scanning near-field optical microscope (SNOM). The x - and y -axis indicate the polarization direction of the incident light. Aluminum nanowires were etched on a silica substrate with a $440 \times 440 \text{ nm}^2$ unit cell.

^{a)}Electronic mail: tsk@orc.soton.ac.uk.

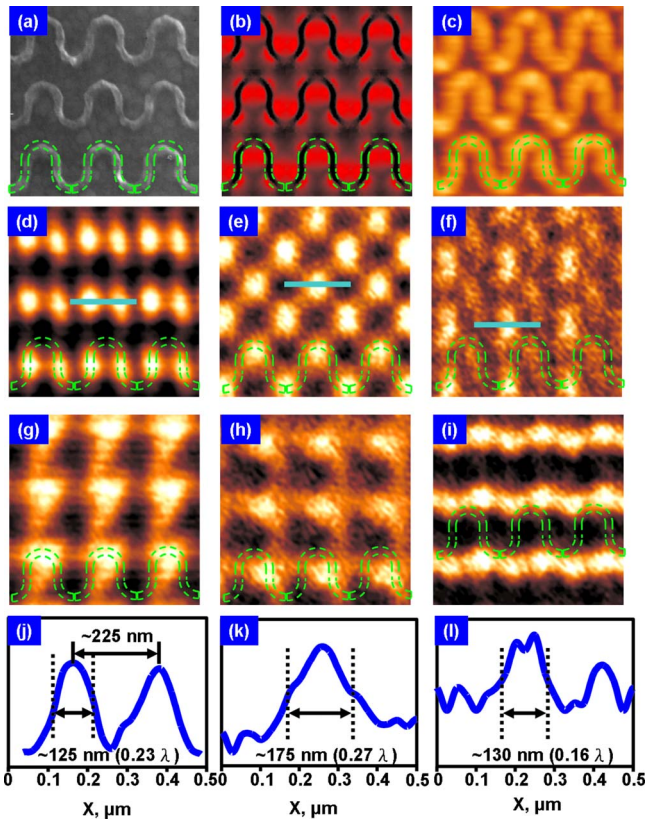


FIG. 2. (Color online) SNOM mapping of a double-periodic nanowire fish-scale array at different wavelengths and polarization. (a) The scanning electron microscope (SEM) image of the nanostructure; (c) the sample topography taken simultaneously with the optical images. The second and third rows show the near-field intensity maps for excitation polarized along (x) and perpendicular (y) to the nanowire meander. Columns correspond to measurements at 550, 660, and 850 nm (from left to right). The bottom row shows field intensity profiles at the position indicated at the x -polarization maps. All maps are $1.32 \times 1.32 \mu\text{m}^2$. (b) The simulated near-field intensity distribution corresponding to the SNOM mapping at the wavelength of 660 nm [plate (e)].

The results of the field mapping for two orthogonal polarizations along and perpendicular to the nanowire meander and for three characteristic wavelengths are shown in Fig. 2 alongside sample topographies taken during the same measurements. They illustrate that the dramatic difference of the field maps is not due to topography-related artifacts¹⁷ but a genuine manifestation of the intrinsic difference in the interaction of the nanostructures with light at different wavelengths and polarizations. The choice of wavelengths used for field mapping is explained in Fig. 3, which shows the experimental transmission spectra of the same sample for x -polarized light (red) and y -polarized light (blue). The x -polarized spectrum has a resonant dip in transmission at around 700 nm linked to the known dipole excitation.^{9,10} The selected wavelengths are therefore on the blue (550 nm) and red (850 nm) wings of the transmission dip and close to its center (660 nm).

One can clearly see that field maps can be controlled by the wavelength and polarization of the incident light. For instance, x -polarized excitation seems to create subwavelength hot-spots with periodic distributions. However, a change of excitation wavelength from 550 to 660 nm dramatically alters the hot-spot pattern as follows: a double periodic arrangement of deeply subwavelength 125 nm hot-spots (0.23λ) located at the vertical sections of the meander

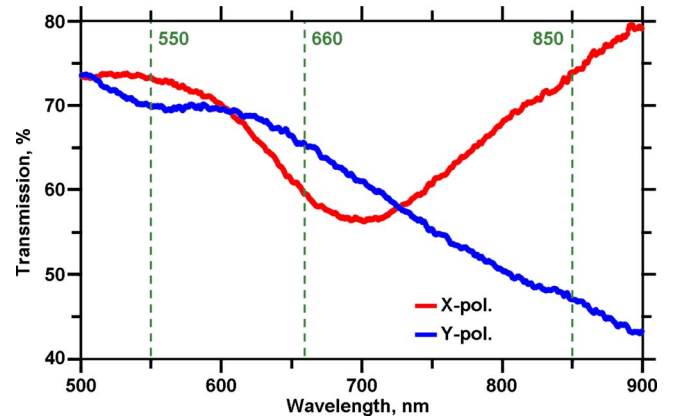


FIG. 3. (Color online) Far-field optical transmission spectra of double-periodic nanowire arrays. The dashed lines indicate the wavelengths used for SNOM mapping of 550, 660, and 850 nm.

pattern observed at 550 nm [plate (d)] becomes, at 660 nm, a single periodic chess-board pattern of somewhat bigger 175 nm hot-spots (0.27λ) located at the peaks and valleys of the meander [plate (e)]. At 850 nm the hot-spots pattern becomes blurred and ill defined [plate (i)]. With vertically polarized excitation at 550 nm the hot-spots seem to be located between the meander rows [plate (g)], moving to the areas between vertical sections of the meander design at 660 nm [plate (h)], and becoming a continuous strip pattern of ill defined spots attached to the vertical sections of the meander at 850 nm [plate (i)].

The nanowire “fish-scale” nanostructure can be considered as a sequence of double-strip line waveguide resonators terminated with a short-circuit section. The full length of the strip within the unit cell, denoted S , is approximately 850 nm. According to previous investigations of fish-scale metamaterials in the microwave region,^{21,22} the wavelength of the array’s resonant response wavelength is linked to the length of the strip resonator; at the main transmission dip the oscillating electric field polarized perpendicular to the direction of the strip (x -polarization) generates a standing wave on the strips with a wavelength, λ_s , that is close to $S/2$. This model also works reasonably for the optical part of the spectrum. Indeed, considering the influence of substrate, the wavelength of excitation in the strip waveguide can be roughly estimated as $\lambda_s \approx \lambda_i / [\sqrt{(\epsilon+1)/2}]$, where λ_i is the wavelength of incident radiation and ϵ is the permittivity of the substrate.²² This estimate gives a value of 533 nm for the incident resonant wavelength for a transparent silica substrate with permittivity $\epsilon=2.1$. Considering that this estimate does not account for cross-unit cell interactions, the finite width and thickness of the strip and losses, it gives a reasonable agreement with the measured value of ~ 700 nm. This perception of the fish-scale metamaterial as a resonant waveguide structure suggests that strong redistribution of the hot-spots caused by changing wavelength and polarization results from a redistribution of the energy in the standing wave. Indeed, away from the resonant wavelength the standing wave pattern must redistribute to accommodate for the mismatch between the waveguide wavelength and the length of the strip inside the unit cell. Moreover, on detuning from the resonance the near-field pattern becomes formed by a superposition of different standing waves linked to various characteristic features of the structure.

Figure 2(b) shows the simulated near-field intensity distribution at the nanowire array at the wavelength of 600 nm for the x -polarized excitation. Here the simulated map shows the field distribution of $|E_x|^2$ in the near-field region. It was calculated using the COMSOL three-dimensional Maxwell equations solver and shows a good agreement with the experimental data [Fig. 2(e)]. We argue that this indicates the influence of the near-field probe does not dramatically change the field distribution and the experimental data may indeed be interpreted as real near-field maps. The ability of the metamaterials to concentrate light at a subwavelength scale is not surprising as the hot-spots are formed by the near-fields with large wave vectors determined by the smallest elements of the metamaterial pattern. What is important, however, is that they can be efficiently and easily controlled by the polarization state and the wavelength of incident radiation.

In conclusion, we demonstrate that subwavelength hot-spot distributions in the metamaterial nanowire landscape can be controlled by the wavelength and polarization of incident radiation. This also demonstrates that metamaterials can be used for tailoring and templating of nanostructured optical fields for experiments such as optical trapping, linear and nonlinear molecular spectroscopy, and Raman scattering.

The authors would like to acknowledge the financial support of the Engineering and Physical Sciences Research Council (U.K.) (Nanoscope: EP/F040644/1 and Portfolio: EP/C511786/1) and the Royal Society.

¹T. W. Ebbesen, H. J. Lezec, H. F. Ghaemi, T. Thio, and P. A. Wolff, *Nature (London)* **391**, 667 (1998).

²N. Papasimakis, V. A. Fedotov, A. S. Schwanecke, N. I. Zheludev, and F. J. Garcia de Abajo, *Appl. Phys. Lett.* **91**, 081503 (2007).

³V. M. Shalaev, W. Cai, U. K. Chettiar, H.-K. Yuan, A. K. Sarychev, V. P. Drachev, and A. V. Kildishev, *Opt. Lett.* **30**, 3356 (2005).

⁴G. Dolling, C. Enkrich, M. Wegener, C. M. Soukoulis, and S. Linden, *Science* **312**, 892 (2006).

⁵A. C. Hryciw, Y. C. Jun, and M. L. Brongersma, *Opt. Express* **17**, 185 (2009).

⁶N. Féridj, J. Aubard, G. Levi, J. R. Krenn, A. Hohenau, G. Schider, A. Leitner, and F. R. Aussenegg, *Appl. Phys. Lett.* **82**, 3095 (2003).

⁷F. M. Huang, N. I. Zheludev, Y. Chen, and F. J. G. de Abajo, *Appl. Phys. Lett.* **90**, 091119 (2007).

⁸F. M. Huang, Y. Chen, F. J. Garcia de Abajo, and N. I. Zheludev, *J. Opt. A, Pure Appl. Opt.* **9**, S285 (2007).

⁹V. A. Fedotov, A. V. Rogacheva, N. I. Zheludev, P. L. Mladyonov, and S. L. Prosvirnin, *Appl. Phys. Lett.* **88**, 091119 (2006).

¹⁰A. S. Schwanecke, V. A. Fedotov, V. V. Khardikov, S. L. Prosvirnin, Y. Chen, and N. I. Zheludev, *J. Opt. A, Pure Appl. Opt.* **9**, L1 (2007).

¹¹A. S. Schwanecke, V. A. Fedotov, V. V. Khardikov, S. L. Prosvirnin, Y. Chen, and N. I. Zheludev, *Nano Lett.* **8**, 2940 (2008).

¹²A. Papakostas, A. Potts, D. M. Bagnall, S. L. Prosvirnin, H. J. Coles, and N. I. Zheludev, *Phys. Rev. Lett.* **90**, 107404 (2003).

¹³S. L. Prosvirnin and N. I. Zheludev, *Phys. Rev. E* **71**, 037603 (2005).

¹⁴J. B. Pendry, *Phys. Rev. Lett.* **85**, 3966 (2000).

¹⁵T. Zentgraf, J. Dorfmueller, C. Rockstuhl, C. Etrich, R. Vogelgesang, K. Kern, T. Pertsch, F. Lederer, and H. Giessen, *Opt. Lett.* **33**, 848 (2008).

¹⁶M. V. Bashevoy, F. Jonsson, K. F. MacDonald, Y. Chen, and N. I. Zheludev, *Opt. Express* **15**, 11313 (2007).

¹⁷B. Hecht, H. Bielefeldt, Y. Inouye, and D. W. Pohl, *J. Appl. Phys.* **81**, 2492 (1997).

¹⁸A. García-Etxarri, I. Romero, F. J. Garcia de Abajo, R. Hillenbrand, and J. Aizpurua, *Phys. Rev. B* **79**, 125439 (2009).

¹⁹P. D. Lacharmoise, N. G. Tognalli, A. R. Goni, M. I. Alonso, A. Fainstein, R. M. Cole, J. J. Baumberg, J. Garcia de Abajo, and P. N. Bartlett, *Phys. Rev. B* **78**, 125410 (2008).

²⁰S. I. Bozhevolnyi, I. I. Smolyaninov, and A. V. Zayats, *Phys. Rev. B* **51**, 17916 (1995).

²¹V. A. Fedotov, P. L. Mladyonov, S. L. Prosvirnin, and N. I. Zheludev, *Phys. Rev. E* **72**, 056613 (2005).

²²S. L. Prosvirnin, S. Tretyakov, and P. L. Mladyonov, *J. Electromagn. Waves Appl.* **16**, 421 (2002).